J. Phys. B: At. Mol. Opt. Phys. **23** (1990) 301-313. Printed in the UK

Absolute ionisation cross sections for electron impact on H_2

H Kossmann, O Schwarzkopf and V Schmidt

Fakultät für Physik, Universität Freiburg, D-7800 Freiburg, West Germany

Received 14 July 1989, in final form 4 September 1989

Abstract. Absolute electron impact cross sections for single ionisation leaving H_2^+ in its electronic ground state and double ionisation leading to dissociation into all four constituents have been determined by a direct method in the energy range 0.15-2.6 keV. The values for single ionisation are in perfect agreement with, but the double-ionisation values are much larger than, the earlier determination by Edwards *et al.* Our results exhibit a close relationship between the H_2 system and its atomic counterpart, helium, with respect to their response to single- and double-ionisation processes.

1. Introduction

The hydrogen molecule provides a unique test case for detailed studies of fragmentation processes because it is the simplest molecule that is both theoretically and experimentally tractable. Thus the results obtained for H_2 offer, in a qualitative manner, the possibility of describing other more complex fragmentation phenomena. In spite of its general interest, cross section values for fragmentation processes in H_2 are rare because they are difficult to assess. The present work concentrates on absolute partial cross sections for two extreme fragmentation processes caused by electron impact, single ionisation leaving H_2^+ in its ground state (cross section $\sigma(H_2^+)$) and double ionisation (cross section $\sigma(H^+, H^+)$) leading to dissociation into all four constituents (four-particle break-up). The only published values for these cross sections are given by Edwards *et al* (1988). In a first step Edwards *et al* determined with the same apparatus and under the same experimental conditions relative cross section values for electron and proton impact on H_2. Absolute cross section values for electron impact were then obtained in a second step: for $\sigma(H_2^+)$ it was necessary to perform calibration measurements also using helium as target gas and to normalise against known absolute values for proton impact (recommended by Rudd *et al* (1985)); for $\sigma(H^+, H^+)$ full account of the experimental conditions was necessary to place this cross section onto an absolute scale, since no other absolute measurements were available.

This paper describes the direct determination of absolute values for both electron impact cross sections, $\sigma(H_2^+)$ and $\sigma(H^+, H^+)$, by the method of time-of-flight ion spectrometry. Apart from belonging to extreme fragmentation processes, both selected cross sections also represent two tempting distinct experimental situations to deal with. For the determination of $\sigma(H_2^+)$ thermal ions have to be analysed and collected; this can be done by standard procedures. However, the determination of $\sigma(H^+, H^+)$ requires a coincidence experiment between ions of appreciable kinetic energy (9.4 eV each (McCulloh and Rosenstock 1968)). Since the dissociation fragments separate with large kinetic energy, the molecular rotation times are long compared with the

0953-4075/90/020301+13$03.50

dissociation times; therefore, the trajectories of the fragment ions will be along the direction of the vibrational motion of the ruptured bond (axial recoil).

The aim of this study is to provide a new set of data for these cross sections. As will be shown below, our $\sigma(H_2^+)$ values are in perfect agreement with, and our $\sigma(H^+, H^+)$ values on the other hand are much larger than, the earlier determination by Edwards *et al* (1988). Furthermore, since our ultimate interest is to study these processes under photon impact, we consider the electron impact experiment as the basis for the development of a proper method for the determination of absolute cross sections.

2. Experimental method

The measurement of the two cross sections is based on counting ions selected by appropriate time-of-flight (TOF) methods. Details about the apparatus will be given elsewhere (Kossmann *et al* 1990). Briefly, the time-of-flight analyser is of the Wiley-McLaren type (Wiley and McLaren 1955) and designed to operate with a periodic start signal and pulsed electric fields. A pulse generator triggers the TOF analyser with a repetition time of 6 μs and synchronously opens the Wehnelt of the electron gun. Within one cycle three phases for the electric field in the target region are realised (cf Kossmann *et al* 1988):

In the first phase, the collection phase of 100 ns duration, the field is set to zero and synchronously the electron beam is switched on, causing ionisation of the hydrogen target. Owing to their initial velocity, the ions leave their place of generation and enlarge the effective source volume that has to be accepted by the analyser.

In the second phase, the acceleration phase of 500 ns duration, the ions are accelerated towards the ion detector (a set of two channelplates). Thermal H_2^+ ions originating from the single-ionisation process will take up a certain velocity depending on the field strength and on the e/m value. Out of all possible pairs of recoiling H^+ ions from double ionisation, only fragment pairs produced with their internuclear axis directed parallel to the axis of the analyser will be selected by the combined action of the acceleration field and suitable diaphragms placed at the end of the second electric field region and in front of the post-acceleration region. Such ion pairs comprise a *forward-* and a *backward-*moving ion. The acceleration field turns the backward ion around by 180°. After the reversal time ΔT_{rev}, the backward ion arrives again at the location it occupied at the instance the electric field was switched on, but now the velocity component parallel to the electric field is forward-directed. Optimum space-focusing (Wiley and McLaren 1955) ensures that for all selected ion pairs the reversal time equals the difference of arrival times at the detector, independent of the time elapsed between the dissociation event and the switching-on time of the acceleration field. The second phase lasts until all H^+ or H_2^+ ions have left the first field region.

During the third phase, which completes the 6.0 μs cycle, slower ions originating from background gas constituents are pushed out of the analyser by reversing the field direction.

Under the conditions described above, the flight times of forward and backward ions are well separated and can be used to set two time windows with respect to the common start pulse of the TOF cycle. The first time window, G_1, accepts only forward-moving ions and provides a start pulse for a time-to-digital converter, which is stopped by the backward-moving ion arriving in the second time window, G_2. Simultaneously,

the H_2^+ ions are counted by setting an appropriate third time window, G_3. An experimental TOF spectrum indicating the three selected time windows is shown in figure 1.

The count rates $I(H_2^+)$ and $I(H^+, H^+)$ for the specified processes are related to the respective cross sections as follows:

$$I(H_2^+) = Nn\sigma(H_2^+)\Delta x\tau(H_2^+)g^k\varepsilon(H_2^+) \tag{1}$$

$$I(H^+, H^+) = Nn\sigma(H^+, H^+)\Delta x\tau(H^+, H^+)g^{2k}\varepsilon(H^+)\varepsilon(H^+) \tag{2}$$

where N is the number of incoming electrons per second, n is the target density, Δx is the length of accepted source volume along the electron beam, $\tau(\cdot)$ is the transmission of the respective processes indicated in parentheses, g^k is the transmission through field-separating meshes, k is the number of meshes and $\varepsilon(\cdot)$ is the detection efficiency of the respective ion indicated in parentheses.

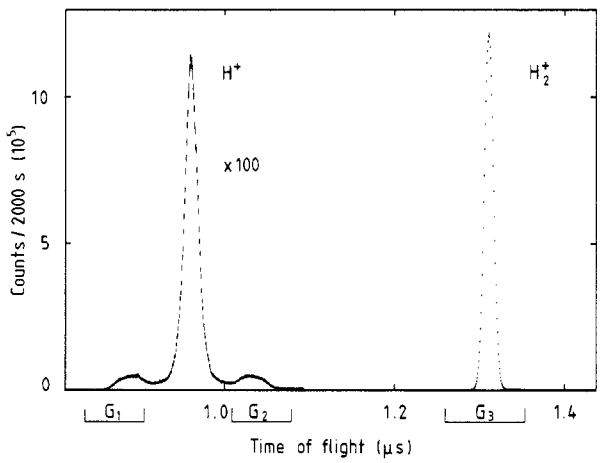

Figure 1. Experimental TOF spectrum showing the H_2^+ peak and, on a different scale, the structured region of H^+ ions originating from various dissociation processes in H_2 and from contributions of the water content in the background gas. Indicated are the gate settings (G_1, G_2) for the coincidence measurement of the H^+ ion pair produced by dissociation of H_2 and the third gate (G_3) for the detection of H_2^+.

The direct determination of the desired cross sections requires knowledge of all constituents in the given formulae, which will be discussed in the next section. In addition we note that special care has to be given to the count rates. During the collection time, more than one ionisation event might occur, especially for H_2^+ production. However, our equipment operates such that, from all ions $I(H_2^+)$ created during the collection time of one cycle, only *one* count will result at most. The connection between the registered count rate $I_{reg}(H_2^+)$ and $I(H_2^+)$ is quoted in Kossmann *et al* (1988).

Since the count rate $I(H^+, H^+)$ is much smaller than $I(H_2^+)$, it is convenient to perform the experiment in three steps. First, the analyser has to be calibrated by measuring $I(He^+)$ and relating it to the known cross section $\sigma(He^+)$, applying equation (1) to helium. Secondly, immediately after the helium measurement, the absolute cross section $\sigma(H_2^+)$ can be determined using equation (1) for H_2^+. However, a higher

accuracy is achieved by evaluating $\sigma(H_2^+)$ from equation (3), which relates the experimental data from the helium and hydrogen measurements in the form of ratios:

$$\frac{I(H_2^+)}{I(He^+)} = \frac{N(H_2)n(H_2)\sigma(H_2^+)\tau(H_2^+)\varepsilon(H_2^+)}{N(He)n(He)\sigma(He^+)\tau(He^+)\varepsilon(He^+)}. \tag{3}$$

Finally the simultaneous measurement of $I(H^+, H^+)$ and $I(H_2^+)$ allows the extraction of $\sigma(H^+, H^+)$ via equation (4), which connects the ratio $I(H^+, H^+)/I(H_2^+)$ of count rates with the cross section ratio:

$$\frac{I(H^+, H^+)}{I(H_2^+)} = \frac{\sigma(H^+, H^+)\varepsilon(H^+)\varepsilon(H^+)\tau(H^+, H^+)g^k}{\sigma(H_2^+)\varepsilon(H_2^+)\tau(H_2^+)}. \tag{4}$$

The latter ratio measurement offers the advantage that in long-term experiments fluctuations in the target density and the electron current cancel out. However, the dependences on ion transmission and detection efficiencies remain. It has to be noted that the coincident detection of the dissociation products brings about a quadratic dependence on the detection efficiency and also on a non-trivial ratio of transmission factors, which demands explicit knowledge of these terms.

3. Experimental details

3.1. Electron beam

The electron beam was generated by a directly heated electron gun producing electrons between 100 and 3000 eV kinetic energy. Pulsing was achieved by capacitive coupling of a positive pulse (approximately +18 V, 10 ns risetime, 100 ns duration) to the Wehnelt, which was kept otherwise on −20 V DC. Typical electron currents were about 0.4 nA. Electron optics produced a beam diameter of less than 2 mm in the interaction region. After traversing the interaction region, the electron beam was trapped in a curved Faraday cup held on +90 V in order to ensure complete charge collection (for details see Nagy *et al* (1980)). The current I_e was measured with a Keithley electrometer (model 602), freshly calibrated by the manufactorer (2% absolute error), and registered using an analogue-to-frequency converter and counter. The number N of incoming electrons per second then follows from $N = I_e/e_0$ with e_0 being the electron charge.

3.2. Target density

Target gas was led into the vacuum chamber producing a homogeneous density distribution. Typical H_2 and helium pressures were approximately 4×10^{-5} mbar, and pressure-dependent effects on the ion signal were found to be negligible. Since the background pressure of 2×10^{-6} mbar cannot be neglected with respect to the target pressure, dissociation processes of the water content in the background gas will contribute to both H_2^+ and H^+ ions. We have proved that the H_2^+ portion is less than 0.3%, which can be neglected, while an essential part of the H^+ signal originates from the background, but no contribution to the *coincident* H^+-H^+ signal was found.

The true value for the target gas density was obtained similar to the procedure described by Nagy *et al* (1980). In short, it is based on the calibration of an ionisation gauge (Leybold IE20) in the 10^{-4} to 10^{-3} mbar range with a Baratron (type 77-M-1) freshly calibrated by the manufactorer (2% absolute error). Via the linearity of the

ionisation gauge, the calibration was then extended down to the target pressure actually used. Proper mounting of the Baratron head and the ionisation gauge with respect to the target region ensured that the pressure at these devices equals the actual pressure in the ionisation region within ±3%. Finally, the target density can be evaluated from the pressure values. Including all error sources, we ascribe to the absolute value of the target density a final error of 8%. However, if only relative values are needed as in equation (3), a smaller error of 4% is appropriate for the ratio of target densities.

3.3. Transmission

Generally, the transmission factors $\tau(H_2^+)$ and $\tau(H^+, H^+)$ depend on the spatial and initial velocity distribution of the ions before the acceleration is turned on as well as on the imaging properties of the TOF analyser. The transmission factors are not directly amenable experimentally. Since the initial velocity distribution is known and the acceleration of the ions is accomplished by homogeneous electric fields, a computer simulation is able to give precise information about the transmission depending on geometry, field strength and time structure needed to resolve the different processes. Moreover, a computer simulation can be utilised to optimise these parameters with respect to resolution and prevention of disturbances caused by other ions.

A reliable check of the outcome of such computer simulations can be achieved by comparing calculated and measured flight times, lineshapes and even complete time-of-flight spectra (cf Kossmann *et al* 1987).

Our computer simulation is a Monte Carlo algorithm well suited for treating the statistical nature of the spatial distribution of the ions in the target gas and their initial velocity distribution. Some idealisations are nevertheless necessary. The incoming electron beam is assumed to be cylindrically shaped with a uniform density; this does not impose a serious constraint as long as the beam diameter is small compared with the size of the first acceleration region. The electric fields, produced by pulses of rectangular shape, are assumed to be homogeneous; this approximation is well fulfilled since different field regions are separated by gold meshes with wire spacing of 0.34 mm (wire diameter 0.02 mm), which is small relative to the length of the field region (greater than 6 mm). The risetime of the voltage pulses is less than 10 ns, again small compared with the pulse duration (for details see Kossmann *et al* (1990)). We note that the transmission of two gold meshes was measured to be $g^2 = 0.75\ (2)$, which compares well with $g^1 = 0.875\ (15)$ following from the optical transmission. Actually, the analyser contains five meshes, giving $g^5 = 0.49\ (2)$.

For thermal ions like H_2^+ and He^+ no discrimination occurs and the transmissions $\tau(H_2^+)$ and $\tau(He^+)$ were calculated to be 0.98 (1) for both ion species.

An algorithm for the energy distribution of the double-ionisation process in H_2 was derived by McCulloh (1968), who also proved its validity experimentally (McCulloh and Rosenstock 1968). The dissociation energy distribution was found to be very broad; appreciable intensity can be expected over a range of 15 eV peaked at 18.8 eV. In the centre-of-mass frame this energy is partitioned in equal parts to the recoiling ionic fragments. In addition, the thermal distribution of the molecules has to be accounted for. Both distributions are included in the calculation of the transmission.

As mentioned in § 2, rectangular diaphragms were inserted to select those ion pairs which fly apart on (or nearly on) the axis of the analyser (forward and backward ions). These diaphragms define an effective solid angle, which increases with decreasing dissociation energy. The maximum size of these diaphragms is limited since otherwise

the minimum time separation of allied ions with smaller dissociation energy would become too short. The requirement of open time windows for the respective H^+ ion pair would then include a large fraction of the nearly thermally distributed ions from the strong peak of the H^+ group (cf figure 1) and therefore increase the accidental coincidences. Computer simulation helped us to optimise the size of our diaphragms with respect to resolution and transmission.

Since the position of the electron beam with respect to the diaphragms can be determined only to an accuracy of ±0.5 mm, we have investigated the influence on $\tau(H^+, H^+)$. For demonstration, figure 2 shows the transmission as a function of the two parameters, distance of beam to diaphragm and deviation of the beam from the middle position of the diaphragm. It is found that $\tau(H^+, H^+) = 6.0(2) \times 10^{-3}$.

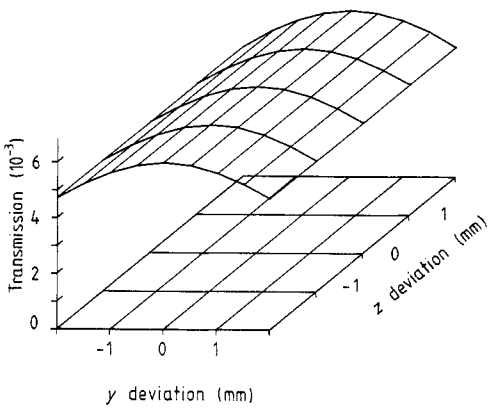

Figure 2. Dependence of the transmission $\tau(H^+, H^+)$ on the position of the incoming electron beam. Nominal position at (0, 0); deviations are given along the z and y directions; the coordinate system xyz is defined by x along the electron beam, y perpendicular to the beam and the TOF analyser axis, and z along the analyser axis.

A calculated flight-time distribution together with an experimental coincidence peak is shown in figure 3. Excellent agreement can be seen. A small background is also visible below 140 ns, which is due to false coincidences. A careful investigation of the behaviour of the background (Schwarzkopf 1989) has shown that the visible false coincidences do not extend into the region of true coincidences and, therefore, can be excluded easily. However, at around 150 ns accidental coincidences contribute and at above 200 ns another background from secondary processes at the channelplate appears. Both these two disturbances were found to be less than 1% of the true coincidence rate.

3.4. Detection efficiency

3.4.1. General. Quantitative information about the absolute detection efficiency of a channelplate system are difficult to assess. The efficiency depends on a variety of parameters: the composition of the particles, their mass, charge and velocity and also on the design of the detector, i.e. the spacing between the two channelplates, the distance between plate and anode, and the electrical operation parameters like voltage across the plates, interplate bias voltage and plate-anode potential difference. The

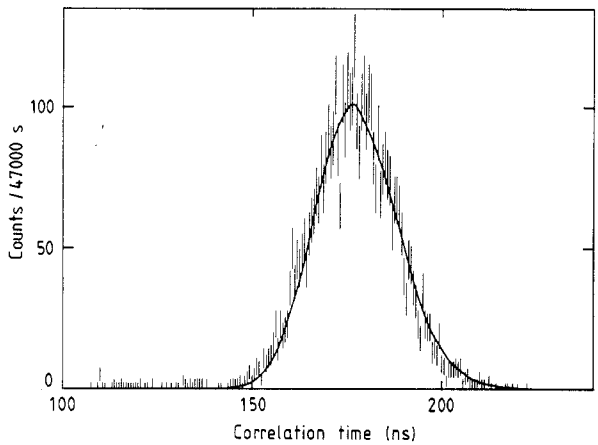

Figure 3. Measured coincidence peak for H^+, H^+ fragmentation following double ionisation of H_2 caused by 400 eV electrons (points with error bars). The timescale shown covers the range of electronically allowed correlation times given by the setting of time windows for forward- and backward-moving ions. The scale is larger than all possible flight-time differences of correlated ion fragments (full curve). The full curve represents the area-adapted computer simulation of the dissociation process.

resulting pulse-height distribution for a detection system always extends to zero pulse height, and hence it is sensitive to the discrimination level of the electronic preamplification system. Moreover, the performance depends on the age of the channelplates, and the gain might vary over the plate surface. Because of these critical dependences on the individual operating conditions, quantitative determination of detection efficiencies is essential.

3.4.2. Relative values. In a first step the pulse-height distribution and the level setting of the discriminator were optimised. Keeping these operation parameters fixed, only the dependence of the detection efficiency on the acceleration field in front of the first plate, i.e. on the ion velocity, remains. Nagy *et al* (1980) showed for channeltrons that the efficiency of all rare-gas ions becomes equal, i.e. independent of mass and charge at high acceleration potentials. To confirm this fact for channelplates and in particular for H^+ (cf Gao *et al* 1984), the relative detection efficiency as a function of the acceleration potential was measured for various ion species. Figure 4 shows the relative detection efficiency of H^+, He^+, Ne^+ and also of H_2^+, normalised to unity at 6.5 kV acceleration potential. The different behaviours can be understood if the velocity and mass dependences of the relative detection efficiencies for the atomic ions and the special behaviour of the molecular ion are taken into account (cf Burrous *et al* 1967, Beuhler and Friedman 1977). The detection efficiency of H^+ and He^+ merges clearly to an asymptotic value, that for Ne^+ ions seems to require even higher acceleration and that for H_2^+ needs special consideration (see below).

3.4.3. Asymptotic value for atoms. In figure 4, each of the ion detection efficiencies was normalised at 6.5 kV to unity, separately. In the following we show that a common asymptotic value exists for He^+ and Ne^+ ions, which can then be applied also for H^+. For this purpose an additional photoionisation experiment was performed at the BESSY electron storage ring, combining ion and electron spectrometry.

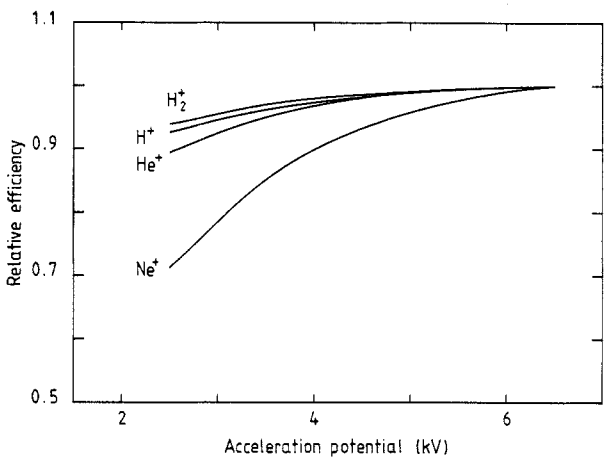

Figure 4. Relative detection efficiencies for H^+, H_2^+, He^+ and Ne^+ ions normalised to unity at 6.5 kV acceleration potential. The measured points were connected by straight lines. All curves were slightly smoothed in order to remove statistical scattering (approximately 1%).

Helium and neon were introduced into the interaction region and He^+ and Ne^+ ions were collected simultaneously, the acceleration voltage being fixed at 6.5 kV. To avoid higher-order contributions and stray light influences from the monochromatised synchrotron light, the ion measurement was performed at 75 eV photon energy. The resulting ion ratio then depends on the ratios of the detection efficiencies, the photoionisation cross sections and on the ratio of target densities, respectively. The cross section ratio is known (absorption data, tabulated by Marr and West (1976), a small correction for the double photoionisation in neon was accounted for).

The target density ratio was evaluated from data obtained by photoelectron spectrometry. To avoid contributions from many-electron processes, a photon energy of 45.08 eV was selected. The angular distribution measurement of He(1s) and Ne(2p) photoelectrons provided the partial photoionisation cross section and target density ratio (cf Kämmerling *et al* 1989). Partial photoionisation cross section values for Ne(2p) and He(1s) are taken from Wuilleumier and Krause (1979) and Marr and West (1976), respectively.

Combining the results of the ion and electron measurements we finally obtained $\varepsilon(He^+, 6.5\,kV)/\varepsilon(Ne^+, 6.5\,kV) = 1.04(8)$. The deviation from the expected value of 1 can be ascribed to the slightly smaller value $\varepsilon(Ne^+, 6.5\,kV)$, since at 6.5 kV the asymptotic value is not yet reached (Nagy *et al* 1980). Since neon is the heaviest ion species in our study, we assume that the lighter atomic ions behave in the same way and take $\varepsilon(H^+, 6.5\,kV)/\varepsilon(He^+, 6.5\,kV) = 1.0$.

3.4.4. Absolute values for atoms. As explained above, it now suffices to fix the absolute detection efficiency for one atomic ion species. For this purpose we studied the single ionisation in helium by electron impact because reliable absolute cross-section data are available for this case, namely the extended compilation of de Heer and Jansen (1977) and the recent investigation of Shah *et al* (1988). Since both data sets deviate slightly by a constant factor, we used for our normalisation procedure the mean value of both cross section data and attribute an error of 5% to it, which covers both data

sets. The ion yield was measured in steps of 200 eV between 200 and 2600 eV, and excellent agreement with the slope of the mean cross section data was found, implying proper normalisation over the whole energy range. Inserting the measured quantities into equation (1) and gathering together the errors for the count rate (0.1%), the absolute electron flux (2%), the absolute target density (8%), the cross section (5%), the calculated transmission (1%) and the transmission of the gold meshes (4%), we finally got $\varepsilon(He^+, 6.5\,kV) = 0.48(7)$. We note that the total uncertainty was obtained by taking the mean value between the square root of the quadratic error sum and the linear sum of the errors in order to account for possible systematic error sources. From $\varepsilon(He^+, 6.5\,kV) = 0.48(7)$, $\varepsilon(H^+, 6.5\,kV)/\varepsilon(He^+, 6.5\,kV) = 1.0$ and the relative detection efficiency (figure 4) it then follows that $\varepsilon(H^+, 3\,kV) = 0.44(7)$.

3.4.5. Absolute value for H_2^+. To extract $\sigma(H_2^+)$ from equation (3) it is necessary to know the ratio $\varepsilon(He^+, 3\,kV)/\varepsilon(H_2^+, 3\,kV)$ of detection efficiencies. It is well known for molecular ions that the fragmentation of the molecule upon impact with the surface yields secondary electron emission induced by each of the fragments, therefore increasing the detection efficiency (Beuhler and Friedman 1977, Burrous *et al* 1967).

The detection efficiency $\varepsilon(atom^+, channel)$ for atoms impinging onto the surface of a single channel of a channelplate detector can be calculated approximately from the zero probability $P(0)$ of secondary electron emission. Since the secondary electron emission obeys a Poisson distribution one gets $\varepsilon(atom^+, channel) = 1 - e^{-\delta}$. Taking into account the open area ratio A_{eff} of a channelplate, which might differ from the geometrical value A because of edge effects, one obtains for the detection efficiency of the channelplate $\varepsilon(atom^+) = A_{eff}(1 - e^{-\delta})$. Our measured value $\varepsilon(H^+, He^+, 6.5\,kV) = 0.48$ can then be explained assuming $A_{eff} = A = 0.55$, yielding $\delta = 2.1$, in perfect agreement with the value deduced from the asymptotic channeltron detection efficiency of Nagy *et al* (1980). This result implies that edge effects are small (cf Sakurai and Hashizume 1987). For channelplates an upper limit for the detection efficiency of H_2^+ can be achieved by allotting the mean secondary electron coefficient δ to each of the fragments (the lower limit is given by $\varepsilon(H_2^+, 6.5\,kV) = 0.48$). One gets $\varepsilon(H_2^+, 6.5\,kV) = 0.54$. Taking the mean between the upper and lower limits, one finally obtains $\varepsilon(H_2^+, 6.5\,kV)/\varepsilon(He^+, 6.5\,kV) = 1.06(6)$ and (see figure 4) $\varepsilon(H_2^+, 3\,kV)/\varepsilon(He^+, 3\,kV) = 1.09(7)$ and $\varepsilon(H_2^+, 3\,kV)/\varepsilon(H^+, 3\,kV) = 1.07(7)$.

4. Results

Our electron impact data for single and double ionisation in H_2 are listed in table 1 and shown in figures 5 and 6 together with other available data. The uncertainty of our values follows from that of the individual contributions in equations (3) and (4), respectively. As overall error to $\sigma(H_2^+)$ and $\sigma(H^+, H^+)$ we ascribe the mean of the linear and quadratic combination of individual errors. For $\sigma(H_2^+)$ this procedure leads to an uncertainty of 13%, for $\sigma(H^+, H^+)$ of 27%. The error for $\sigma(H_2^+)$ comprises the absolute cross section $\sigma(He^+)$ with 5% and diverse ratios from the relative measurement, in particular the statistical error of count rates (0.1%), the electron flux ratio (2%), the target density ratio (4%) and the ratio of detection efficiencies (6%). In the error analysis for $\sigma(H^+, H^+)$, the detection efficiency ratio was combined with $\sigma(H_2^+)$ and substituted by the remaining quantities of equation (3) because then the dependence on $\varepsilon(H_2^+)$ cancels and the error of $\sigma(H_2^+)\varepsilon(H_2^+)/\varepsilon(H^+)$ amounts to 9% only. For the

Table 1. Compilation of electron impact data for ionisation processes in H_2.

Electron energy (eV)	$\sigma(H_2^+)$[a] (Mb)	$\sigma_{90}(H^+, H^+)$[b] (kb)	σ_{ion}[c] (Mb)
100	70.3		92.4
150	67.5	291	81.2
175	65.3[d]	296	
200	63.2	329	71.4
225	59.3[d]	291	
250	55.7	284	
300	47.3	250	57.4
350	43.1	221	
400	39.5	211	47.6
500	33.8	167	40.6
600	29.2		35.6
700	26.6	120	31.6
750			30.0
800	23.9		28.3
900	21.8		26.0
1000	20.0	77	24.0
1200	17.3		
1400	15.3		
1500	14.4[d]	51	
1600	13.7		
1800	12.4		
2000	11.4	40	
2200	10.5		13.3
2400	9.8		
2500	9.4[d]	30	
2600	9.12		
3000	8.09		

[a] This work, total uncertainty 13%.
[b] This work, total uncertainty 27%; the lower index 90 indicates that the measurements were performed at 90° with respect to the electron beam.
[c] From van Wingerden *et al* (1980), total uncertainty 6%.
[d] Interpolated values.

only. For the remaining quantities in equation (4) we have 3% statistical error on the counting rates, 15% on $\varepsilon(H^+)$, 1% on $\tau(H_2^+)$, 3.3% on $\tau(H^+, H^+)$ and 4% for g[5].

Before discussing the results we would like to comment on the effect of a possible ion angular distribution on our cross section values. Since *all* thermal ions from the source volume are collected, such effects have no impact on the cross section $\sigma(H_2^+)$. However, since our TOF analyser accepts the dissociative ion pairs only at a mean angle of 90° with respect to the incoming electron beam, we characterise in table 1 our double-ionisation cross section $\sigma(H^+, H^+)$ with the lower index 90. Only if the dissociative ion pair has no angular distribution does $\sigma_{90}(H^+, H^+)$ equal $\sigma(H^+, H^+)$. According to Edwards *et al* (1988; for electron impact) and Yousif *et al* (1988; for proton impact) such angular distribution effects should be small. However, Dunn and Kieffer (1963) and Van Brunt and Kieffer (1970) found for electron energies below a few hundred electronvolts a pronounced angle dependence for fragmentation into H and H^+, which might give some evidence for an angle-dependent double-ionisation process at low impact energies. An angle dependence is supported also by our investigation of double photoionisation in H_2, which shows for photon energies below 110 eV a pronounced

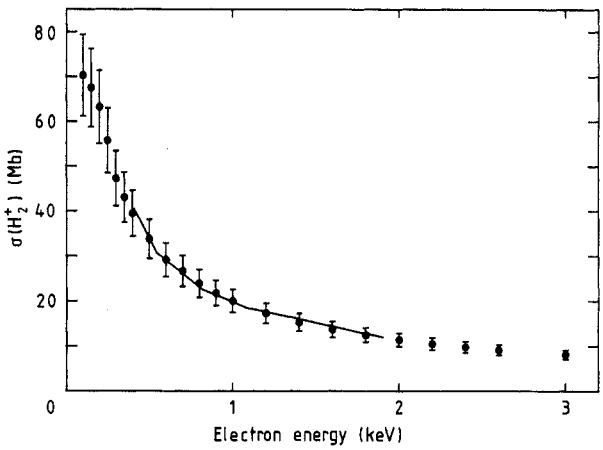

Figure 5. Absolute electron impact cross section $\sigma(H_2^+)$ for single ionisation: full circles with error bars, this work; full curve, Edwards *et al* (1988).

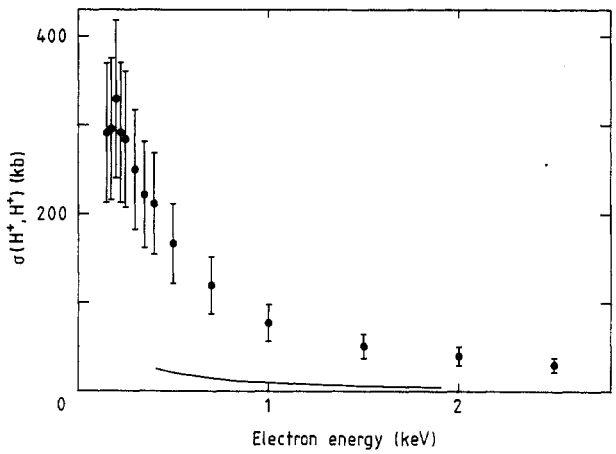

Figure 6. Absolute electron impact cross sections $\sigma(H^+, H^+)$ for double ionisation: full circles with error bars, this work; full curve, Edwards *et al* (1988). The data of Edwards *et al* are shown without error bars.

angle dependence (Kossmann *et al* 1989). However, this must not be in contradiction to a weak angle dependence in electron impact at high energies since the kinematics of electron impact allows a wide range for energy and momentum transfer, which usually diminishes angular distribution effects. Nevertheless, our $\sigma_{90}(H^+, H^+)$ values might differ from $\sigma(H^+, H^+)$ in the low-energy region.

In figure 5 our $\sigma(H_2^+)$ values are compared with those of Edwards *et al* (1988). The data of Edwards *et al* (1988) are shown without error bars (the authors state for their values an error of approximately 5%, the proton reference data are reliable to within 10%). Both data sets are in excellent agreement.

Figure 6 shows our $\sigma(H^+, H^+)$ values together with those of Edwards *et al* (1988). Here a discrepancy by a factor of approximately 8 can be seen. Such a discrepancy can originate only in an erroneous determination of the constituents of equations (2) or (4). Recent measurements of the target pressure have questioned the absolute values

of Edwards *et al* (1988) but the relative values will not change (Edwards *et al* 1989). In fact, the relative shape agrees with our data.

Total ionisation cross sections σ_{ion} for electron impact on the hydrogen molecule have been compiled by van Wingerden *et al* (1980); see also de Heer and Inokuti (1985). Comparing our cross sections with these data (cf table 1), one observes that $\sigma(H_2^+)$ amounts to approximately 83(10)% of σ_{ion} leaving 17(10)% for all dissociation processes, which is larger than the value of about 7% given by Rapp *et al* (1965) for ions with kinetic energies above 2.5 eV.

5. Conclusions

The new set of experimental data for electron impact ionisation leading to the bound ground state of H_2^+ is in excellent agreement with the earlier results; that of the double-ionisation cross section $\sigma(H^+, H^+)$ is found to be substantially larger than previously stated. As a consequence, the ratio of double- to all single-ionisation processes turns out to be much larger. By comparing this ratio with the corresponding one for helium, the same magnitude can be recognised. On the other hand, the cross section for single ionisation leaving H_2^+ ions in their ground state is approximately twice that of He^+. The different magnitudes of the ionisation cross sections probably reflect differences in the one-centre atomic and two-centre molecular structure; it might be revealed by proper theoretical treatment. For electron impact ionisation, therefore, the H_2 system behaves roughly like its atomic counterpart, helium.

Acknowledgments

The authors thank M Menendez for helpful comments on the manuscript and A K Edwards for communicating his recent results prior to publication (Edwards *et al* 1989). The support by the Forschungsschwerpunkt FR-NW-34 of the University of Freiburg and the funds by the German Federal Minister for Research and Technology (BMFT, Contract No 05372AAIB) for the experiments at BESSY are gratefully acknowledged.

References

Beuhler R J and Friedman L 1977 *Int. J. Mass Spectrom. Ion Phys.* **23** 81-97

Burrous C N, Lieber A J and Zaviantseff V T 1967 *Rev. Sci. Instrum.* **38** 1477-81

de Heer F J and Inokuti M 1985 *Electron Impact Ionization* ed T D Märk and G H Dunn (New York: Springer) pp 232-76

de Heer F J and Jansen R H J 1977 *J. Phys. B: At. Mol. Phys.* **10** 3741-58

Dunn G H and Kieffer L J 1963 *Phys. Rev.* **132** 2109-17

Edwards A K, Wood R M, Beard A S and Ezell R L 1988 *Phys. Rev.* A **37** 3697-701

Edwards A K, Wood R M, Davis J L and Ezell R L 1989 *Nucl. Instrum. Methods* B **40(4)** 174-7

Gao R S, Gibner P S, Newman J H, Smith K A and Stebbings R F 1984 *Rev. Sci. Instrum.* **55** 1756-9

Kämmerling B, Kossmann H and Schmidt V 1989 *J. Phys. B: At. Mol. Opt. Phys.* **22** 841-54

Kossmann H, Kämmerling B, Menzel T, Schäuble B, Schwarzkopf O and Schmidt V 1987 *BESSY Jahresbericht* unpublished

Kossmann H, Krässig B and Schmidt V 1988 *J. Phys. B: At. Mol. Opt. Phys.* **21** 1489-97

Kossmann H, Schwarzkopf O, Kämmerling B and Schmidt V 1989 *Phys. Rev. Lett.* **63** 2040-3

Kossmann H, Schwarzkopf O, Krässig B and Schmidt V 1990 to be published
McCulloh K E 1968 *J. Chem. Phys.* **48** 2090-3
McCulloh K E and Rosenstock H M 1968 *J. Chem. Phys.* **48** 2084-9
Marr G W and West J B 1976 *At. Data Nucl. Data Tables* **18** 497-508
Nagy P, Skutlartz A and Schmidt V 1980 *J. Phys. B: At. Mol. Phys.* **13** 1249-67
Rapp D, Englander-Golden P and Briglia D D 1965 *J. Chem. Phys.* **42** 4081-5
Rudd M E, Kim Y-K, Madison D H and Gallagher J W 1985 *Rev. Mod. Phys.* **57** 965-94
Sakurai T and Hashizume T 1987 *Rev. Sci. Instrum.* **52** 236-9
Schwarzkopf O 1989 *Diplom-Thesis* Freiburg University, unpublished
Shah M B, Elliott D S, McCallion P and Gilbody H B 1988 *J. Phys. B: At. Mol. Phys.* **21** 2751-61
Van Brunt R J and Kieffer L J 1970 *Phys. Rev.* A **2** 1293-304
van Wingerden B, Wagenaar R W and de Heer F J 1980 *J. Phys. B: At. Mol. Phys.* **13** 3481-91
Wiley W C and McLaren I M 1955 *Rev. Sci. Instrum.* **26** 1150-7
Wuilleumier F and Krause M O 1979 *J. Electron Spectrosc. Relat. Phenom.* **15** 15-20
Yousif F D, Lindsay B G and Latimer C J 1988 *J. Phys. B: At. Mol. Opt. Phys.* **21** 4157-64